NANO LETTERS

pubs.acs.org/NanoLett

Letter

Unveiling the Electronic Structure of Grain Boundaries in Anatase with Electron Microscopy and First-Principles Modeling

James A. Quirk,*,△ Bin Miao,△ Bin Feng, Gowoon Kim, Hiromichi Ohta, Yuichi Ikuhara, and Keith P. McKenna*

Cite This: *Nano Lett.* 2021, 21, 9217−9223

Read Online

ACCESS | Metrics & More | Article Recommendations | Supporting Information

ABSTRACT: Polycrystalline anatase titanium dioxide has drawn great interest, because of its potential applications in high-efficiency photovoltaics and photocatalysts. There has been speculation on the electronic properties of grain boundaries but little direct evidence, because grain boundaries in anatase are challenging to probe experimentally and to model. We present a combined experimental and theoretical study of anatase grain boundaries that have been fabricated by epitaxial growth on a bicrystalline substrate, allowing accurate atomic-scale models to be determined. The electronic structure in the vicinity of stoichiometric grain boundaries is relatively benign to device performance but segregation of oxygen vacancies introduces barriers to electron transport, because of the development of a space charge region. An intrinsically oxygen-deficient boundary exhibits charge trapping consistent with electron energy loss spectroscopy measurements. We discuss strategies for the synthesis of polycrystalline anatase in order to minimize the formation of such deleterious grain boundaries.

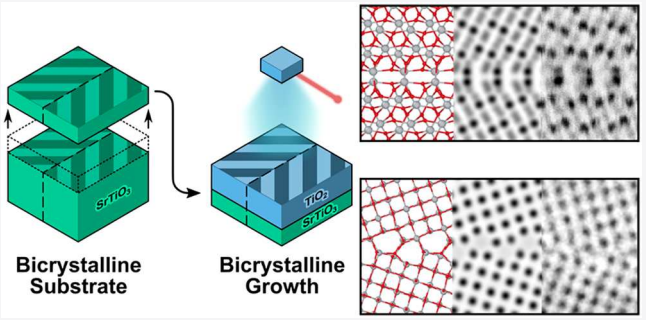

KEYWORDS: *Grain Boundaries, Titanium Dioxide, Density Functional Theory, Electron Microscopy, Space Charge*

The anatase phase of titanium dioxide (TiO_2) finds a wide range of energy-related applications, including as charge transport layers in photovoltaic devices,[1,2] photocatalysts for hydrogen production,[3,4] and as battery electrode materials.[5−7] For most practical applications, anatase TiO_2 is prepared in nanoparticle form, before hydrothermal coarsening or sintering to produce a nanoporous film.[8,9] Such materials are technologically desirable, because of their high surface-area-to-volume ratio, which increases the accessible surface area for the adsorption of reactants in photocatalytic applications and allows for more efficient charge injection from contacting solar-absorber materials in photovoltaic applications. For example, the current world's leading lead halide perovskite solar cells (>25% efficiency) employ nanoporous anatase TiO_2 as an electron transport layer.[10] While surfaces play a significant part in technological applications, polycrystalline materials unavoidably contain large numbers of grain boundaries (GBs), which are expected to play a decisive role in determining their electronic properties. For example, GBs can be associated with a local change in the band gap of a material and can introduce traps for charge carriers.[11,12] Charge trapping can be seriously detrimental to the performance of devices, because it decreases carrier mobility and increases the likelihood of carrier recombination, leading to decreased current and decreased efficiency in applications. GBs can also negatively impact efficiency, because of the segregation of charged point defects, which can give rise to a space charge region affecting carrier transport near the boundary.[13,14] Transient photocurrent measurements have shown that carrier diffusion and recombination in polycrystalline anatase is significantly affected by the average size of nanoparticles in the sample.[15,16] However, changing nanoparticle size in nanoporous materials affects the cross-sectional area of GBs, their total number, and the total surface area. Therefore, it is extremely challenging to experimentally disentangle the combined roles of point defects, surfaces, and GBs in polycrystalline anatase, with the various models proposed in the literature.[15−19] Without a good understanding of GBs in anatase, devising effective methods to reduce charge trapping and increase mobility has proven very difficult.

Given the challenges associated with performing experiments to directly address GB properties in anatase, one can turn to computational modeling to provide insight and predictions at the atomic scale. The defacto standard of computational electronic structure methods is density func-

Received: August 11, 2021
Published: November 1, 2021

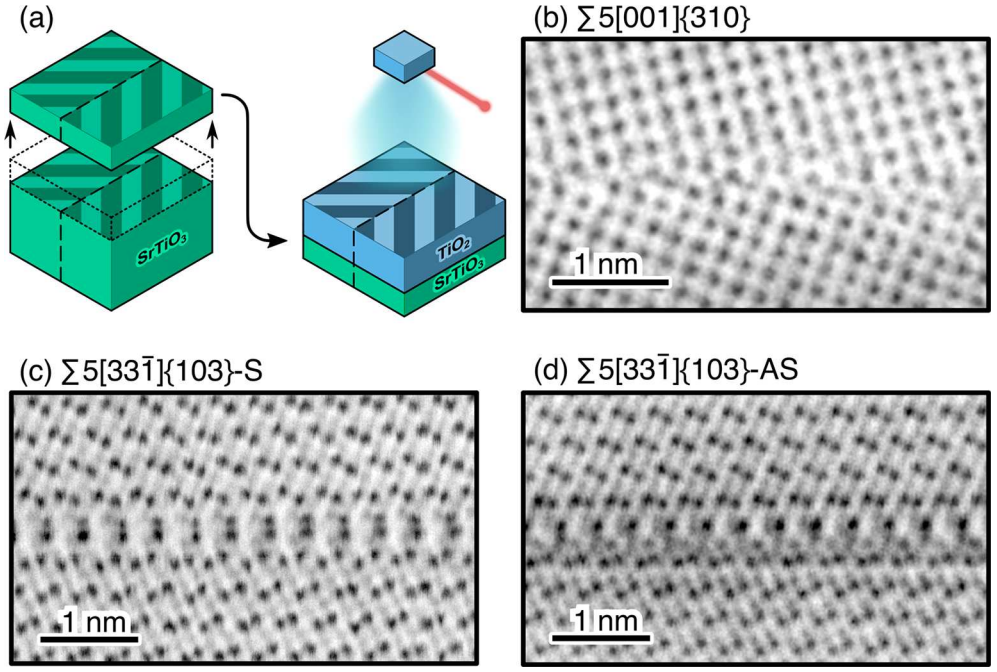

Figure 1. (a) Schematic diagram showing how a slice of an $SrTiO_3$ bicrystal is used as a substrate for the growth of anatase via pulsed laser deposition. The orientation of the anatase grains are templated by the orientation of the grains in the substrate. ABF STEM images of the (b) Σ5[001]{310} GB, (c) Σ5[33$\bar{1}$]{103}-S GB, and (d) Σ5[33$\bar{1}$]{103}-AS GB also are shown.

tional theory (DFT), because of its low computational cost and reasonable accuracy. However, accurate modeling of charge trapping remains challenging, requiring the careful application of methods such as hybrid DFT, where some fraction of exact Fock exchange is incorporated into standard semilocal DFT, in order to correctly capture the behavior of localized charges.[20−23] Predicting the atomic structure of GB defects is also difficult, because of the large number of degrees of freedom involved and the fact that GB structures realized in practice are often metastable.[24,25] Therefore, it is desirable to directly confirm first-principles predictions of a GB structure experimentally so that prediction of corresponding electronic properties can be made with confidence. As discussed above, this is challenging for anatase GBs; therefore, to date, the only intergrain defect that has been characterized experimentally is the low-energy and high-symmetry Σ3{112} twin boundary, which forms fortuitously by oriented attachment during hydrothermal coarsening of anatase nanoparticles.[26] This conundrum concerning the role of internal interfaces is a common one in modern materials science, and it requires the combined efforts of theory and experiment to resolve.

Here, we tackle this problem for Σ5 GBs in anatase by combining aberration-corrected scanning transmission electron microscopy (STEM) with a hybrid DFT functional containing 10.5% Fock exchange, a value which is optimized to accurately describe charge trapping in bulk anatase.[22] The standard bicrystal approach for fabricating and imaging GBs[24,27−29] is inaccessible for anatase as large single crystals irreversibly transform to the rutile phase if annealed at temperatures above 600 °C.[26,30] As an alternative, we prepare a well-defined Σ5[001]{310} $SrTiO_3$ bicrystal[28] from which we cut a suitable substrate onto which an anatase TiO_2 film can be grown epitaxially. The orientation of the grains in the substrate templates the orientation of the grains in the growing anatase film, which, in turn, encourages the formation of GBs (Figure 1a). We characterize the Σ5{310} and the Σ5[33$\bar{1}$]{103} GBs (the latter is observed due to the proposed formation of {112} twins in the anatase film). Computational models of stable GB configurations are determined by systematic scans through different rigid-body translations that are possible between the grains, yielding structures and simulated STEM images that are in excellent agreement with experiment. We find that the Σ5[001]{310} and Σ5[33$\bar{1}$]{103} GBs generally only weakly perturb the electronic structure of anatase and should be relatively benign for conductivity. However, segregation of ionized oxygen vacancies is predicted to lead to a space charge region and an intergrain electrostatic barrier to electron transport of ∼0.1 eV. We also predict a highly oxygen-deficient variant of the Σ5[33$\bar{1}$]{103} GB that contains large numbers of electron traps in the vicinity of the boundary. This is supported by electron energy-loss spectroscopy (EELS) measurements that the region in the vicinity of the Σ5[33$\bar{1}$]{103} GB is more reduced than the bulklike region of the grains. The increased number of electron traps in the vicinity of the GB will lead to decreased carrier mobility and increased rates of recombination, which would be seriously detrimental to the performance in photovoltaics, photocatalysis, and rechargeable battery applications.

Two distinct GB orientations are observed in the annular bright-field (ABF) STEM images of the anatase bicrystal. The GB structures are shown in Figures 1b−d, where the dark contrast corresponds to Ti and O columns. The first is the expected Σ5[001]{310} GB (Figure 1b), which corresponds to the orientation of the $SrTiO_3$ bicrystal substrate. We also observe Σ5[33$\bar{1}$]{103} GBs, which we propose are present due to the intersection of Σ3{112} twin boundaries, which form in the anatase grains (see Figure S1 in the Supporting Information). For the Σ5[33$\bar{1}$]{103}, we observe two different configurations in the experimental images: one that is symmetric about the boundary plane, which we label the Σ5[33$\bar{1}$]{103}-S (Figure 1c), and another that is asymmetric, which we label the Σ5[33$\bar{1}$]{103}-AS (Figure 1d).

https://doi.org/10.1021/acs.nanolett.1c03099
Nano Lett. 2021, 21, 9217−9223

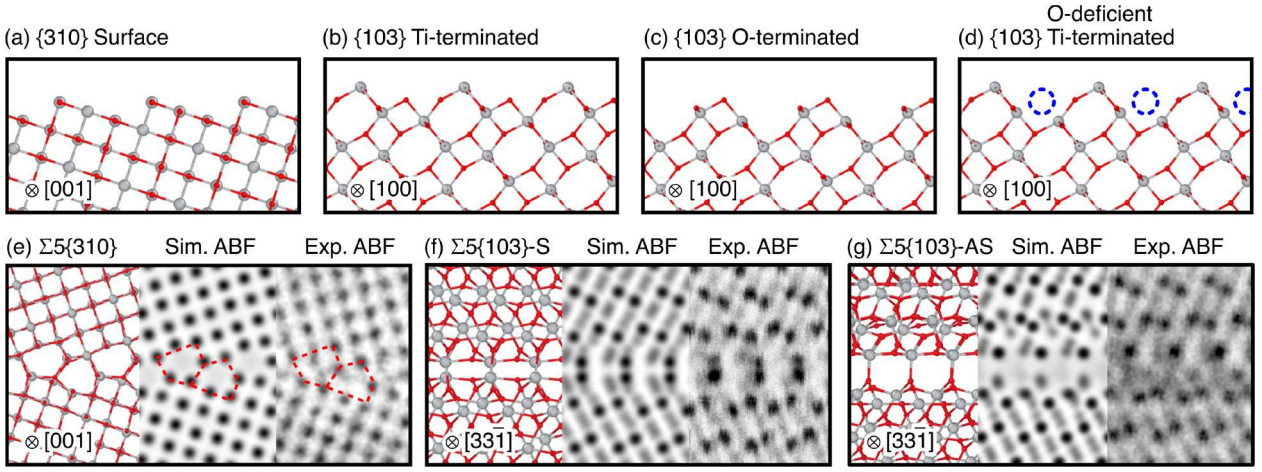

Figure 2. Structural models for the surface termination of grains: (a) {310}, (b) Ti-terminated {103}, (c) O-terminated {103}, and (d) O-deficient Ti-terminated {103}. In all structural models, large gray spheres are titanium and small red spheres are oxygen. The projections for each view are given in the bottom left of each panel. Also shown are corresponding simulated and experimental ABF STEM images for the (e) Σ5{310}, (f) Σ5{103}-S, and (g) Σ5{103}-AS GBs.

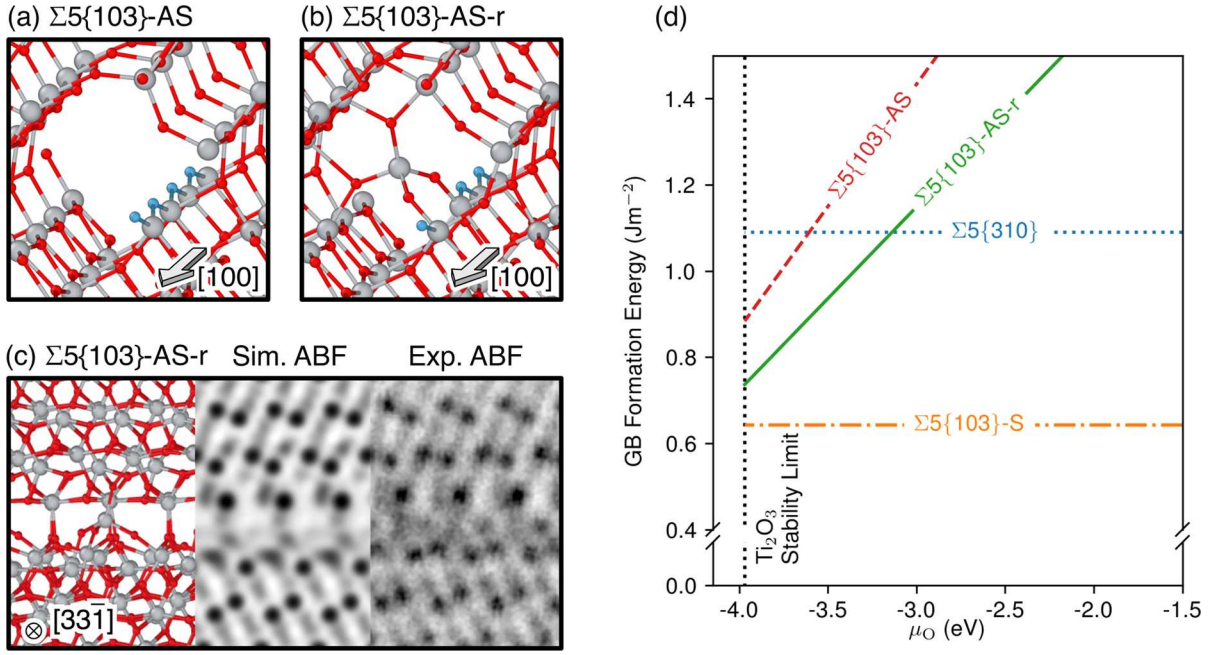

Figure 3. Structural models of the (a) Σ5{103}-AS and (b) Σ5{103}-AS-r GBs. Large gray spheres are titanium, small red spheres are oxygen, and bridging O atoms have been highlighted in blue. Projection indicated by arrows in bottom right of panels. (c) Structural model of the Σ5{103}-AS-r GB with corresponding simulated and experimental ABF STEM images. (d) Formation energies of the GBs, as a function of the oxygen chemical potential, μ_O, showing that, in the O-poor limit, the Σ5{103}-AS-r GB has a similar formation energy to the Σ5{103}-S GB. Note that the full of range μ_O up to the oxygen-rich limit of μ_O = 0.0 eV is not shown.

We utilize procedures that are commonly employed to model GBs, by building a periodic supercell containing two symmetrically equivalent GBs separated by a sufficient distance to ensure that the two GBs do not interact with each other.[31−33] Further details can be found in the Supporting Information. These periodic models are constructed by adjoining two grains, which can have different surface terminations. We identify only one inequivalent termination for the {310} grain (Figure 2a) and our Σ5{310} GB model is constructed by combining two grains with this termination. For the {103} grain, we find three plausible surface terminations leading to several GB models. The symmetric Σ5{103}-S GB is constructed from two Ti-terminated grains (Figure 2b). The combination of two O-terminated grains yields very high formation energies and was not considered further. The asymmetric Σ5{103}-AS GB can be constructed by combining an O-terminated grain (Figure 2c) and an oxygen-deficient Ti-terminated grain (Figure 2d). The removal of oxygen from the Ti-terminated grain is necessary to eliminate the unphysical dipole between the grains that otherwise forms. This oxygen-deficient surface termination has been observed experimentally in STEM studies of anatase nanorods.[34]

For each GB, we identify the most stable structures by performing a series of geometry optimizations at the different rigid-body translations possible between the grains and

https://doi.org/10.1021/acs.nanolett.1c03099
Nano Lett. 2021, 21, 9217−9223

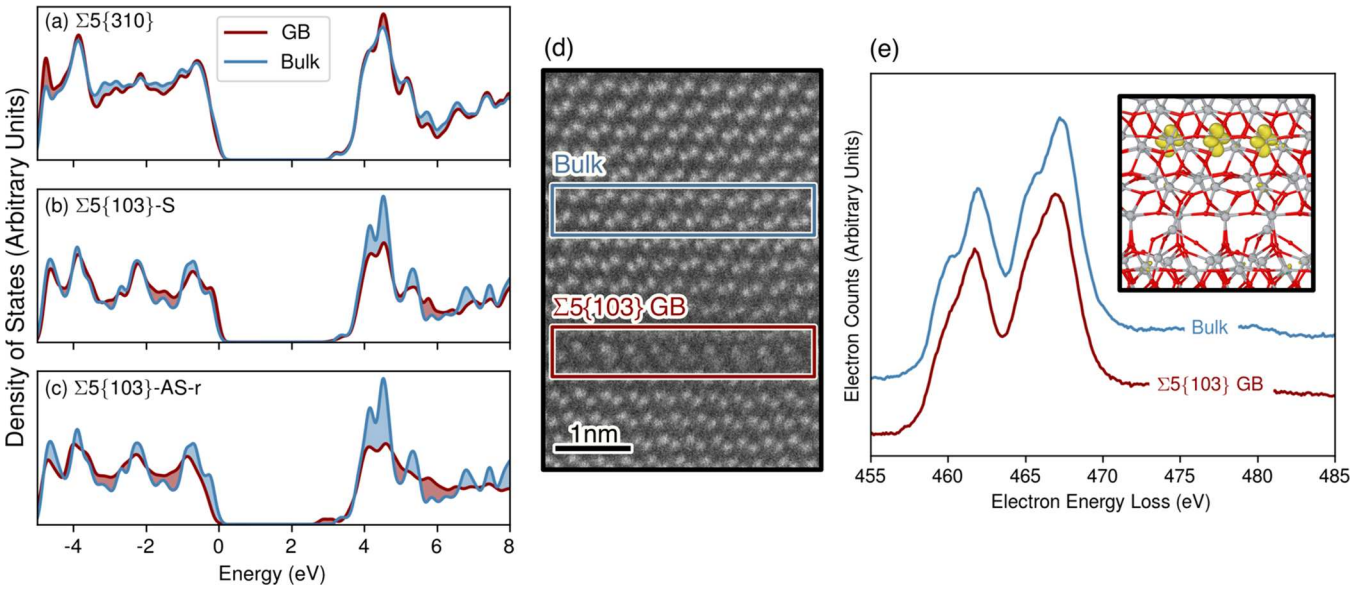

Figure 4. Projected density of states for the (a) Σ5{310}, (b) Σ5{103}-S, and (c) Σ5{103}-AS-r GBs. For each plot, energy is relative to the valence band maximum, the blue curve represents the bulklike region, and the red curve represents the GB region. The shaded portions indicate where a region has more states of a given energy. For the Σ5{310} and Σ5{103}-S GBs, no states appear in the gap, but for the Σ5{103}-AS-r GB states appear at ∼0.5 eV below the conduction band minimum. (d) STEM image with boxes showing regions corresponding to electron energy-loss spectroscopy (EELS) spectra. (e) EELS spectrum for the bulklike region and the Σ5{103}-S GB region showing the Ti $L_{2,3}$ edge. Curves have been offset vertically for clarity. Note that, in the GB region, the two doublets are replaced by two broad peaks, indicating increased presence of Ti^{3+}. The image shown in the top right is the absolute spin density isosurface (displayed at 0.05 a_0^{-3}) associated with electrons trapped in the vicinity of the Σ5{103}-S GB.

calculating a formation energy (see the Supporting Information). This approach has been successful in predicting grain-boundary structures in various materials.[27,28,32] We find two inequivalent minima for the Σ5{310} GB with almost identical formation energies of 1.03 and 1.09 J m^{-2}. Simulated ABF STEM images were produced for both of these structures, and the best agreement is found with the higher formation energy structure (Figure 2e). When two GB structures are very close in energy, it is not unusual for the predicted lowest energy GB structures to not appear in experimental samples and similar behavior is reported in a study of Σ5{310} GBs in magnesium oxide.[24] Our further simulations and analysis of electronic structure shall focus on the GB, which shows better agreement with the experiment. For the Σ5{103}-S GB, we determine one distinct minima that corresponds to a small formation energy of 0.64 J m^{-2}. The simulated ABF STEM image produced for this structure is in excellent agreement with experimental observations (Figure 2f). Our nonstoichiometric Σ5{103}-AS structure is missing 8 O atoms per GB in the simulation supercell, meaning that its formation energy is dependent on the chemical potential of oxygen (μ_O). In the oxygen-poor limit (see Supporting Information), our Σ5{103}-AS structure has a formation energy of 0.91 J m^{-2} and the simulated ABF STEM image shows good agreement with experimental observations, in terms of the dark contrast corresponding to columns of titanium (Figure 2g), but shows less agreement in terms of the contrast in the GB core.

In the Σ5{103}-AS GB model, there are rows of "bridging" O atoms that have their bonds strained by ∼12% (Figure 3a), with bonding that is analogous to the unreconstructed {001} anatase surface. For the {001} surface, this strain is relieved by a well-characterized (1 × 4) reconstruction, where every fourth bridging oxygen atom is replaced by a TiO_3 unit.[35] We attempt a similar reconstruction at the GB, which we label Σ5{103}-AS-r, where we replace every fourth bridging oxygen with a TiO_4 unit (Figure 3b). This reconstruction reduces the strain on the bridging oxygen atoms to ∼4%. When comparing simulated ABF STEM images with the experimental image, the Σ5{103}-AS-r model, we see that the there is still good agreement, in terms of the positions of the columns of titanium but, with the addition of the TiO_4 units, there are darker regions within the GB core, which is in better qualitative agreement than the Σ5{103}-AS model (Figure 3c). In the oxygen-poor limit of μ_O, the Σ5{103}-AS-r has a formation energy of 0.74 J m^{-2}, which is significantly lower than that of our predicted Σ5{310} structure or the Σ5{103}-AS structure (see Figure 3d). Given the good agreement with the experimental image and the lower formation energy, our further analysis of electronic properties shall focus on the Σ5{103}-AS-r structure.

In order to understand the electronic structure of the GBs, projected density of states (PDOS) for atoms in the vicinity of the GBs were calculated and compared with a bulklike region far from the boundary plane. Neither the Σ5{310} nor the Σ5{103}-S exhibit significantly altered band gaps or any states within the gap (Figures 4a and 4b), which indicates that these GBs do not present deep charge traps in their equilibrium geometry. We verify this by explicitly adding electrons and holes, finding that holes delocalize over oxygen sites near the GBs and electrons delocalize over titanium sites in the bulklike regions of the grains. For the oxygen-deficient Σ5{103}-AS-r, we see states appearing at ∼0.5−1.0 eV below the conduction band minimum (Figure 4c), corresponding to electron traps (i.e., Ti^{3+} species, as seen in the inset in Figure 4d). EELS measurements were performed on the Σ5{103} GB region to confirm this prediction (scanned regions are shown in Figure 4d). We found the Σ5{103}-S structure is unstable under the electron beam so only the results of Σ5{103}-AS are presented

https://doi.org/10.1021/acs.nanolett.1c03099
Nano Lett. 2021, 21, 9217−9223

(shown in Figure 4e). The EELS spectra for the Σ5{103}-AS GB show that the two doublets associated with the Ti^{4+} $L_{3,2}$ edges in bulk anatase are replaced with the two broad peaks in the vicinity of the GB. Based on previous studies, which compare Ti $L_{3,2}$ edges in TiO_2 and Ti_2O_3,[36] this is indicative of a higher proportion of Ti^{3+}, compared to the bulklike region. The box scan area for EELS analysis is shown in Figure 4e. On the other hand, EELS results indicate that no electron trapping occurs for the Σ5{310} GB (see Figure S3 in the Supporting Information).

After determining electronic and atomic structures, we investigated the properties of oxygen vacancies in the vicinity of the Σ5{310} and Σ5{103}-S GBs (see the Supporting Information). We do not find any vacancy sites where is it favorable for excess electrons to trap. Instead, the vacancies behave as they do in the bulk, where electrons preferentially delocalize into the conduction band. However, we do find that there is a drive for vacancies to segregate to the boundary with some sites being more favorable in the vicinity of the GB than in the bulklike region by 0.92 and 0.35 eV for the Σ5{310} and Σ5{103}-S GBs, respectively. Segregation of charged defects to GBs leads to the development of a space charge region, which, for the Σ5{310} and Σ5{103}-S, we estimate to introduce small potential barriers on the order of 0.1 eV for the transport of charge carriers across the boundaries (see the Supporting Information). For the Σ5{103}-AS and Σ5{103}-AR-r GBs, it is not straightforward to define a meaningful segregation energy as the structures are intrinsically defective. However, if we calculate the space charge potential that would correspond to the relevant layer to be entirely vacant of oxygen, then we see that this would correspond to a space charge barrier of ∼0.15 eV, which would also be detrimental to charge mobility in addition to the presence of predicted charge traps.

Our results predict that the pristine Σ5{310} and Σ5{103}-S GB structures would be fairly benign for the performance of anatase in photovoltaic and photocatalytic applications. The GBs show no indication of charge traps in their equilibrium geometry, nor do we predict that oxygen vacancies at the GBs would favorably trap electrons, although they would introduce a small space charge potential barrier. In contrast, the oxygen-deficient Σ5{103}-AS and Σ5{103}-AS-r GBs would be far more pathological for device performance; the structure inherently contains large numbers of oxygen vacancies and under-coordinated Ti sites. We find that the excess electrons trap on under-coordinated Ti sites, which is consistent with a previous theoretical study using the same functional investigating the properties of highly oxygen-deficient anatase nanoparticles.[37] Vacancies that strongly trap electrons at the GB would reduce the number of mobile carriers introduced by each vacancy, reduce electron mobility, and could lead to increased carrier recombination, leading to reduced conductivity in photovoltaic applications. On the other hand, these trap states appear at ∼0.5−1.0 eV below the conduction band minimum and would increase visible-light absorption. This is beneficial for photocatalytic applications and is supported by experiments that show oxygen-deficient anatase samples have higher photocatalytic performance.[38,39]

These results provide insight into how the properties of GBs in anatase may be engineered to mitigate undesirable electron trapping. In the nanocrystalline anatase films employed in devices, GBs are formed when two nanoparticle surfaces come into contact and attach during sintering or hydrothermal coarsening. Defects present at the surfaces of the precursor nanoparticles should influence the resulting GB structure. For example, it is known that GBs can form through oriented attachment of nanoparticles along minority facets during hydrothermal coarsening. This process has been identified as being responsible for the formation of Σ3{112} twin boundaries in nanocrystalline anatase.[26] As stated previously, experimental observations have shown that {103} surfaces appear as oxygen-deficient minority facets in anatase nanoparticles, alongside surfaces such as {102}.[34] We suggest that, in the event that a GB forms through attachment along highly oxygen-deficient minority facets, it could be the case that a nonstoichiometric, oxygen-deficient structure similar to the Σ5{103}-AS or Σ5{103}-AS-r GBs may form. Anatase is typically oxygen-deficient and it is not straightforward to control the degree of oxygen deficiency at surfaces or the quantities of minority facets present prior to sintering or coarsening. However, it would be possible to treat the surface of the nanoparticles with beneficial dopants so that these dopants can then become incorporated into the GBs. For example, a beneficial dopant might act as an electron donor, to fill charge traps introduced by nonstoichiometry. For less-reduced GBs, which we predict do not introduce deep traps, it may be preferential to seek a dopant that would mitigate the formation of a space charge, either by acting as an oppositely charged defect or by discouraging the segregation of oxygen vacancies to the GBs.

In summary, we present a combined experimental and computational investigation into the atomic and electronic structure of Σ5{310} and Σ5{103} GBs in anatase TiO_2. Low-energy structures predicted by the first-principles models show excellent agreement with experimental observations, as evidenced by simulated ABF STEM images. Analysis of the electronic structure indicates that the Σ5{310} GB would be relatively benign for the performance of photovoltaic or photocatalytic devices, because it does not present electron traps in its equilibrium geometry. For the Σ5{103} GB, however, we find two different GB structures. A stoichiometric structure that shows no electrons traps in equilibrium geometry and another, oxygen-deficient variant, which we predict to contain a significant number of trapped electrons. These predictions are supported by EELS, which shows the Σ5{103} GB to be more reduced than the bulklike regions of the grain. Our predictions of the lack of significant perturbation near the pristine Σ5{310} and Σ5{103}-S GBs may provide some explanation as to why polycrystalline anatase shows excellent performance in applications. However, our prediction of the pathological charge-trapping behavior of the oxygen-deficient Σ5{103}-AS GBs highlights the need to consider the effects that chemical potential and growth conditions may have on the formation of highly defective and nonstoichiometric boundaries. Mitigating these deleterious effects, e.g., via directed doping of the nanoparticle surfaces prior to sintering, should improve carrier mobility and reduce recombination leading to improved performance for applications in photovoltaics, photocatalysis, and rechargeable batteries.

■ ASSOCIATED CONTENT

Supporting Information

The Supporting Information is available free of charge at https://pubs.acs.org/doi/10.1021/acs.nanolett.1c03099.

https://doi.org/10.1021/acs.nanolett.1c03099
Nano Lett. 2021, 21, 9217−9223

Proposed formation mechanism of Σ5{103} GBs through twinning during grain growth; grain-boundary formation energy as a function of translation between grains; oxygen vacancy segregation energies and space charge profile; experimental details of sample growth and imaging; computational details of pseudopotentials, *k*-point sampling, and cutoff energies (PDF)

AUTHOR INFORMATION

Corresponding Authors

James A. Quirk − *Department of Physics, University of York, Heslington, York YO10 5DD, United Kingdom;* orcid.org/0000-0003-3581-1615; Email: jaq502@york.ac.uk

Keith P. McKenna − *Department of Physics, University of York, Heslington, York YO10 5DD, United Kingdom;* orcid.org/0000-0003-0975-3626; Email: keith.mckenna@york.ac.uk

Authors

Bin Miao − *Institute of Engineering Innovation, University of Tokyo, Bunkyo-ku, Tokyo 113-8656, Japan; State Key Laboratory of Reliability and Intelligence of Electrical Equipment, Hebei University of Technology, Tianjin 300130, China*

Bin Feng − *Institute of Engineering Innovation, University of Tokyo, Bunkyo-ku, Tokyo 113-8656, Japan;* orcid.org/0000-0002-4306-2979

Gowoon Kim − *Graduate School of Information Science and Technology, Hokkaido University, Kita, Sapporo 060-0814, Japan;* orcid.org/0000-0002-5803-839X

Hiromichi Ohta − *Research Institute for Electronic Science, Hokkaido University, Sapporo 001-0020, Japan;* orcid.org/0000-0001-7013-0343

Yuichi Ikuhara − *Advanced Institute for Materials Research, Tohoku University, Aoba-ku, Sendai 980-8577, Japan; Institute of Engineering Innovation, University of Tokyo, Bunkyo-ku, Tokyo 113-8656, Japan; Nanostructures Research Laboratory, Japan Fine Ceramics Center, Atsuta-ku, Nagoya 456-8587, Japan;* orcid.org/0000-0003-3886-005X

Complete contact information is available at: https://pubs.acs.org/10.1021/acs.nanolett.1c03099

Author Contributions

△J.A.Q. and B.M. contributed equally to this manuscript.

Notes

The authors declare no competing financial interest.

ACKNOWLEDGMENTS

A part of this work was supported by the Japan Society for the Promotion of Science (JSPS) KAKENHI (Grant Nos. JP17H06094, JP19H05788, JP19H05791), and the "Nanotechnology Platform" by Ministry of Education, Culture, Sports, Science, and Technology in Japan (MEXT). K.McK. acknowledges support from EPSRC (Nos. EP/K003151/1, EP/P006051/1, and EP/P023843/1). This work made use of the facilities of Archer, the UK's national high-performance computing service, via our membership in the UK HPC Materials Chemistry Consortium, which is funded by EPSRC (Nos. EP/L000202, EP/R029431). This work also made use of the Viking Cluster, which is a high-performance computer facility provided by the University of York. All data created during this research are available by request from the University of York Research database (DOI: 10.15124/af2d144a-8b00-4808-85a0-0cef636098cc).

REFERENCES

(1) O'Regan, B.; Grätzel, M. A Low-Cost, High-Efficiency Solar Cell Based on Dye-Sensitized Colloidal TiO_2 Films. *Nature* **1991**, *353*, 737.

(2) Bai, Y.; Mora-Sero, I.; De Angelis, F.; Bisquert, J.; Wang, P. Titanium Dioxide Nanomaterials for Photovoltaic Applications. *Chem. Rev.* **2014**, *114*, 10095−10130.

(3) Fujishima, A.; Honda, K. Electrochemical Photolysis of Water at a Semiconductor Electrode. *Nature* **1972**, *238*, 37.

(4) Kumar, S. G.; Devi, L. G. Review on Modified TiO_2 Photocatalysis Under UV/visible Light: Selected Results and Related Mechanisms on Interfacial Charge Carrier Transfer Dynamics. *J. Phys. Chem. A* **2011**, *115*, 13211−13241.

(5) Kavan, L.; Grätzel, M.; Rathouský, J.; Zukalb, A. Nanocrystalline TiO_2 (Anatase) Electrodes: Surface Morphology, Adsorption, and Electrochemical Properties. *J. Electrochem. Soc.* **1996**, *143*, 394.

(6) Xu, Y.; Memarzadeh Lotfabad, E.; Wang, H.; Farbod, B.; Xu, Z.; Kohandehghan, A.; Mitlin, D. Nanocrystalline Anatase TiO_2: a New Anode Material for Rechargeable Sodium Ion Iatteries. *Chem. Commun.* **2013**, *49*, 8973−8975.

(7) Ortiz, G. F.; Hanzu, I.; Djenizian, T.; Lavela, P.; Tirado, J. L.; Knauth, P. Alternative Li-Ion Battery Electrode Based on Self-Organized Titania Nanotubes. *Chem. Mater.* **2009**, *21*, 63−67.

(8) Medri, V.; Servadei, F.; Bendoni, R.; Natali Murri, A.; Vaccari, A.; Landi, E. Nano-to-Macroporous TiO_2 (Anatase) by Cold Sintering Process. *J. Eur. Ceram. Soc.* **2019**, *39*, 2453−2462.

(9) Krtil, P.; Fattakhova, D.; Kavan, L.; Burnside, S.; Grätzel, M. Lithium Insertion Into Self-Organized Mesoscopic TiO_2 (Anatase) Electrodes. *Solid State Ionics* **2000**, *135*, 101−106.

(10) Jeong, J.; et al. Pseudo-Halide Anion Engineering for α-$FAPbI_3$ Perovskite Solar Cells. *Nature* **2021**, *592*, 381−385.

(11) Wei, J.; Ogawa, T.; Feng, B.; Yokoi, T.; Ishikawa, R.; Kuwabara, A.; Matsunaga, K.; Shibata, N.; Ikuhara, Y. Direct Measurement of Electronic Band Structures at Oxide Grain Boundaries. *Nano Lett.* **2020**, *20*, 2530−2536.

(12) Tong, C.-J.; McKenna, K. P. Passivating Grain Boundaries in Polycrystalline CdTe. *J. Phys. Chem. C* **2019**, *123*, 23882−23889.

(13) De Souza, R. A. The Formation of Equilibrium Space-Charge Zones at Grain Boundaries in the Perovskite Oxide $SrTiO_3$. *Phys. Chem. Chem. Phys.* **2009**, *11*, 9939−9969.

(14) Feng, B.; Lugg, N. R.; Kumamoto, A.; Ikuhara, Y.; Shibata, N. Direct Observation of Oxygen Vacancy Distribution Across Yttria-Stabilized Zirconia Grain Boundaries. *ACS Nano* **2017**, *11*, 11376−11382.

(15) Nakade, S.; Matsuda, M.; Kambe, S.; Saito, Y.; Kitamura, T.; Sakata, T.; Wada, Y.; Mori, H.; Yanagida, S. Dependence of TiO_2 Nanoparticle Preparation Methods and Annealing Temperature on the Efficiency of Dye-Sensitized Solar Cells. *J. Phys. Chem. B* **2002**, *106*, 10004−10010.

(16) Nakade, S.; Saito, Y.; Kubo, W.; Kitamura, T.; Wada, Y.; Yanagida, S. Influence of TiO_2 Nanoparticle Size on Electron Diffusion and Recombination in Dye-Sensitized TiO_2 Solar Cells. *J. Phys. Chem. B* **2003**, *107*, 8607−8611.

(17) Cai, J.; Han, L. Theoretical Investigation on Interfacial-Potential-Limited Diffusion and Recombination in Dye-Sensitized Solar Cells. *J. Phys. Chem. C* **2011**, *115*, 17154−17162.

(18) Cao, F.; Oskam, G.; Meyer, G. J.; Searson, P. C. Electron Transport in Porous Nanocrystalline TiO_2 Photoelectrochemical Cells. *J. Phys. Chem.* **1996**, *100*, 17021−17027.

(19) Dloczik, L.; Ileperuma, O.; Lauermann, I.; Peter, L.; Ponomarev, E.; Redmond, G.; Shaw, N.; Uhlendorf, I. Dynamic Response of Dye-Sensitized Nanocrystalline Solar Cells: Character-

ization by Intensity-Modulated Photocurrent Spectroscopy. *J. Phys. Chem. B* **1997**, *101*, 10281−10289.
(20) Becke, A. D. A New Mixing of Hartree-Fock and Local Density-Functional Theories. *J. Chem. Phys.* **1993**, *98*, 1372−1377.
(21) Zhang, Y.; Yang, W. A Challenge for Density Functionals: Self-Interaction Error Increases for Systems With a Noninteger Number of Electrons. *J. Chem. Phys.* **1998**, *109*, 2604−2608.
(22) Elmaslmane, A. R.; Watkins, M. B.; McKenna, K. P. First-Principles Modeling of Polaron Formation in TiO_2 Polymorphs. *J. Chem. Theory Comput.* **2018**, *14*, 3740−3751.
(23) Elmaslmane, A.; Wetherell, J.; Hodgson, M.; McKenna, K.; Godby, R. Accuracy of Electron Densities Obtained via Koopmans-Compliant Hybrid Functionals. *Phys. Rev. Mater.* **2018**, *2*, 040801.
(24) Yan, Y.; Chisholm, M.; Duscher, G.; Maiti, A.; Pennycook, S.; Pantelides, S. Impurity-Induced Structural Transformation of a MgO Grain Boundary. *Phys. Rev. Lett.* **1998**, *81*, 3675.
(25) Wang, Z.; Saito, M.; McKenna, K. P.; Ikuhara, Y. Polymorphism of Dislocation Core Structures at the Atomic Scale. *Nat. Commun.* **2014**, *5*, 3239.
(26) Penn, R. L.; Banfield, J. F. Formation of Rutile Nuclei at Anatase {112} Twin Interfaces and the Phase Transformation Mechanism in Nanocrystalline Titania. *Am. Mineral.* **1999**, *84*, 871−876.
(27) Nishimura, H.; Matsunaga, K.; Saito, T.; Yamamoto, T.; Ikuhara, Y. Atomic Structures and Energies of Σ7 Symmetrical Tilt Grain Boundaries in Alumina Bicrystals. *J. Am. Ceram. Soc.* **2003**, *86*, 574−80.
(28) Imaeda, M.; Mizoguchi, T.; Sato, Y.; Lee, H.-S.; Findlay, S.; Shibata, N.; Yamamoto, T.; Ikuhara, Y. Atomic Structure, Electronic Structure, and Defect Energetics in [001](310) Σ5 Grain Boundaries of $SrTiO_3$ and $BaTiO_3$. *Phys. Rev. B: Condens. Matter Mater. Phys.* **2008**, *78*, 245320.
(29) Schusteritsch, G.; Ishikawa, R.; Elmaslmane, A.; Inoue, K.; McKenna, K.; Ikuhara, Y.; Pickard, C. Anatase-Like Grain Boundary Structure in Rutile Titanium Dioxide. *Nano Lett.* **2021**, *21*, 2745−2751.
(30) Hanaor, D. A.; Sorrell, C. C. Review of the Anatase to Rutile Phase Transformation. *J. Mater. Sci.* **2011**, *46*, 855−874.
(31) McKenna, K. P. Structure, Electronic Properties, and Oxygen Incorporation/Diffusion Characteristics of the Σ5 TiN (310)[001] Tilt Grain Boundary. *J. Appl. Phys.* **2018**, *123*, 075301.
(32) Bean, J. J.; McKenna, K. P. Origin of Differences in the Excess Volume of Copper and Nickel Grain Boundaries. *Acta Mater.* **2016**, *110*, 246−257.
(33) Quirk, J. A.; Lazarov, V. K.; McKenna, K. P. Electronic Properties of {112} and {110} Twin Boundaries in Anatase TiO_2. *Adv. Theory Simul.* **2019**, *2*, 1900157.
(34) Yuan, W.; Meng, J.; Zhu, B.; Gao, Y.; Zhang, Z.; Sun, C.; Wang, Y. Unveiling the Atomic Structures of the Minority Surfaces of TiO_2 Nanocrystals. *Chem. Mater.* **2018**, *30*, 288−295.
(35) Lazzeri, M.; Selloni, A. Stress-Driven Reconstruction of an Oxide Surface: the Anatase TiO_2 (001)-(1× 4) Surface. *Phys. Rev. Lett.* **2001**, *87*, 266105.
(36) Lusvardi, V.; Barteau, M.; Chen, J. G.; Eng, J., Jr; Frühberger, B.; Teplyakov, A. An NEXAFS Investigation of the Reduction and Reoxidation of TiO_2 (001). *Surf. Sci.* **1998**, *397*, 237−250.
(37) Quirk, J. A.; Lazarov, V. K.; McKenna, K. P. First-Principles Modeling of Oxygen-Deficient Anatase TiO_2 Nanoparticles. *J. Phys. Chem. C* **2020**, *124*, 23637−23647.
(38) Justicia, I.; Ordejón, P.; Canto, G.; Mozos, J. L.; Fraxedas, J.; Battiston, G. A.; Gerbasi, R.; Figueras, A. Designed Self-Doped Titanium Oxide Thin Films for Efficient Visible-Light Photocatalysis. *Adv. Mater.* **2002**, *14*, 1399−1402.
(39) Wei, S.; Ni, S.; Xu, X. A New Approach to Inducing Ti^{3+} in Anatase TiO_2 for Efficient Photocatalytic Hydrogen Production. *Chin. J. of Catal.* **2018**, *39*, 510−516.

https://doi.org/10.1021/acs.nanolett.1c03099
Nano Lett. 2021, 21, 9217−9223